A STUDY OF THE INNERMOST REGION OF THE AGN USING RANDOM FOREST REGRESSOR

NAKARIN MANKATWIT

A Thesis Submitted in Partial Fulfillment of the Requirements for the

Degree of Master of Science in Physics

Suranaree University of Technology

Academic Year 2022

การศึกษาสภาวะแวดล้อม ณ ใจกลางกาแล็กซีกัมมันต์โดยใช้การวิเคราะห์ถดถอยแบบแรนดอมฟอเรสต์

นายนครินทร์ มั่นเขตรวิทย์

วิทยานิพนธ์นี้เป็นส่วนหนึ่งของการศึกษาตามหลักสูตรปริญญาวิทยาศาสตรมหาบัณฑิต
สาขาวิชาฟิสิกส์
มหาวิทยาลัยเทคโนโลยีสุรนารี
ปีการศึกษา 2565

A STUDY OF THE INNERMOST REGION OF THE AGN USING RANDOM FOREST REGRESSOR

Suranaree University of Technology has approved this thesis submitted in partial fulfillment of the requirements for a Master's Degree.

Thesis Examining Committee

Wasutep Luangtip

(Asst. Prof. Dr. Wasutep Luangtip)

Chairperson

Poemwai Chainakun

(Asst. Prof. Dr. Poemwai Chainakun)

Member (Thesis Adviser)

Tirawut Worrakitpoonpon

(Asst. Dr. Tirawut Worrakitpoonpon)

Member

Ittipol Fongkaew

(Dr. Ittipol Fongkaew)

Member

Chatchai Jothityangkoon

(Assoc. Prof. Dr. Chatchai Jothityangkoon)

Vice Rector for Academic Affairs

and Quality Assurance

Santi Maensiri

(Prof. Dr. Santi Maensiri)

Dean of Institute of Science

นครินทร์ มั่นเขตรวิทย์ : การศึกษาสภาวะแวดล้อม ณ ใจกลางกาแล็กซีกัมมันต์โดยใช้การวิเคราะห์ถดถอยแบบแรนดอมฟอเรสต์ (A STUDY OF THE INNERMOST REGION OF THE AGN USING RANDOM FOREST REGRESSOR) อาจารย์ที่ปรึกษา : ผู้ช่วยศาสตราจารย์ ดร.เพิ่มวัย ชัยนะกุล, 44 หน้า.

คำสำคัญ: กาแล็กซีกัมมันต์, จานพอกพูนมวล, โคโรนารังสีเอกซ์, การวิเคราะห์ถดถอยแบบแรนดอมฟอเรสต์

เราได้พัฒนาแมชชีนเลิร์นนิง โดยเฉพาะการวิเคราะห์ถดถอยแบบแรนดอมฟอเรสต์เพื่อทำนายระยะห่างของโคโรนารังสีเอกซ์กับหลุมดำในนิวเคลียสกาแล็กซีกัมมันต์โดยใช้ข้อมูลจำลองของความหนาแน่นสเปกตรัมพลังงานในการฝึกฝนและตรวจสอบความแม่นยำ จากนั้นใช้แบบจำลองการวิเคราะห์ถดถอยแบบแรนดอมฟอเรสต์ที่ได้นี้ทำการศึกษาวิวัฒนาการของโคโรนาในกาแล็กซีกัมมันต์สองระบบคือ IRAS 13224-3809 และ 1H 0707-495 ที่สังเกตการณ์ด้วยกล้องโทรทัศน์ XMM-Newton ความหนาแน่นสเปกตรัมพลังงานจำลองนั้นถูกสร้างขึ้นในรูปแบบ power-law ซึ่งมีช่วงความถี่และช่วงสัญญาณที่คล้ายกับข้อมูลที่สังเกตได้จริง จากนั้นความหนาแน่นสเปกตรัมพลังงานเหล่านี้จะถูกรวมเข้ากับฟังก์ชันการตอบสนองของจานพอกพูนมวลจากแบบจำลอง Lamp-post และจะถูกใช้ในการฝึกและทดสอบแบบจำลองการวิเคราะห์ถดถอยแบบแรนดอมฟอเรสต์เพื่อทำนายระยะห่างของโคโรนา แบบจำลองที่ทดสอบด้วยชุดข้อมูลความหนาแน่นสเปกตรัมพลังงานจำลองมีประสิทธิภาพสูงโดยมีค่า $R^2 \sim 0.93$ จากนั้นใช้แบบจำลองนี้ทดสอบกับความหนาแน่นสเปกตรัมพลังงานที่ได้จากการสังเกตการณ์จริง โดยลบช่วงความถี่บางส่วนที่ถูกครอบงำโดยสัญญาณรบกวนปัวซองออก เราพบว่าแบบจำลองสามารถรองรับการลบช่องความถี่ได้มากถึง 10 ช่อง ในขณะที่ยังคงความแม่นยำในการทำนายสูง ($R^2 > 0.9$) และความแม่นยำของแบบจำลองนั้นยังเพิ่มขึ้นเมื่อสัดส่วนการสะท้อนเพิ่มขึ้นอีกด้วย จากนั้นใช้แบบจำลองการวิเคราะห์ถดถอยแบบแรนดอมฟอเรสต์นี้เพื่อทำนายความสูงโคโรนาของกาแล็กซีกัมมันต์ทั้งสอง และพบว่าโคโรนามีการเคลื่อนที่ระหว่างความสูงในช่วง ~5–18 r_g เหนือหลุมดำโดยมีค่า $R^2 > 0.9$ สำหรับชุดข้อมูลที่ได้การสังเกตการณ์จริงทั้งหมด และเรายังพบอีกด้วยว่าแม้ว่ามวลของหลุมดำจะแตกต่างประมาณ 10% จากค่าที่ถูกฝึกฝนแบบจำลองยังคงมีความแม่นยำสูง โดยสรุปนั้นแบบจำลองการวิเคราะห์ถดถอยแบบแรนดอมฟอเรสต์

ที่ถูกพัฒนาขึ้นนี้รองรับสมมติฐานที่ว่าโคโรนานั้นมีการเปลี่ยนแปลงความสูง โดยที่ความสูงมี
ความสัมพันธ์กับกำลังส่องสว่างของกาแล็กซีกัมมันต์ทั้งสองที่ใช้ในการศึกษานี้

สาขาวิชาฟิสิกส์   ลายมีชื่อนักศึกษา_____

ปีการศึกษา 2565   ลายมือชื่ออาจารย์ที่ปรึกษา_____

NAKARIN MANKATWIT : A STUDY OF THE INNERMOST REGION OF THE AGN USING RANDOM FORREST REGRESSOR. THESIS ADVISOR : ASST. PROF. POEMWAI CHAINAKUN, Ph.D. 44 PP.

Keyword: active galaxies, accretion disc, X-ray corona, random forest regressor

We have developed a machine learning model, specifically a random forest regressor (RFR), to predict the coronal height in active galactic nuclei (AGNs) using simulated power spectral density (PSD) data. We then applied this model to study the corona evolution in two AGNs, IRAS 13224-3809 and 1H 0707-495, observed by XMM-Newton. The simulated PSDs were produced in a power-law form with a frequency range and bins similar to those of the observed data. These PSDs were convolved with relativistic disc-response functions from a lamp-post source, and then used to train and test the RFR model to predict the coronal height. The model with the simulated PSD data set has high performance, with $R^2 \sim 0.93$. Then applied the RFR model to the observed PSDs where some bins dominated by Poisson noise were removed. The model can support up to ~10 bin removals while maintaining a prediction accuracy of $R^2 > 0.9$. The accuracy also increased with the reflection fraction. The coronal heights of both AGNs, were varying between ~5–18 r_g above the black hole, with $R^2 > 0.9$ for all observations. Even if the true mass differed by 10% from the trained value, the model still achieved high accuracy. Finally, we found that the model supports height-changing corona, where the height is correlated to the source luminosity in both AGNs.

School of Physics

Academic Year 2022

Student's Signature_____

Advisor's Signature_____

ACKNOWLEDGEMENTS

CONTENTS

CONTENTS (Continued)

LIST OF TABLES

LIST OF FIGURES

LIST OF FIGURES (Continued)

LIST OF FIGURES (Continued)

LIST OF FIGURES (Continued)

LIST OF ABBREVIATIONS

AGN	Active Galactic Nuclei
SMBH	Supermassive Black Hole
RFR	Random Forest Regression
ISCO	Innermost Stable Circular Orbit
$M_\odot$	Solar Mass
R_f	Reflection Fraction

CHAPTER I

INTRODUCTION

Active Galactic Nuclei (AGNs) emit electromagnetic radiation across a broad range of wavelengths, from radio to Gramma bands. And all AGNs have the same fundamental composition: a supermassive black hole at the center, surrounded by a disc or ring of dust known as an accretion disc or torus. The variations observed in the appearance of AGNs stem from our vantage point on Earth, which alters how we perceive the black hole and its surrounding accretion disc, as shown in Figure 1.1. However, it is believed that the accretion disc or another component itself cannot produce hard X-rays. Recent research indicates that the X-ray radiation is generated by the corona, located in the innermost region of the AGN (Haardt and Maraschi, 1991; Kara et al., 2016). There is an ongoing debate about the geometry and evolution of the corona, and it is still unclear how the corona connects to the disc and transforms into relativistic jets (Reynolds and Nowak, 2003).
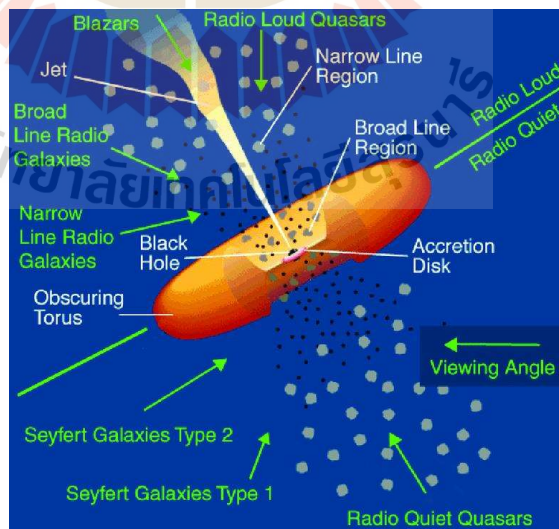
Figure 1.1 The standard unified AGN model, AGN with different names depends on what can be seen in the observer's orientation (Urry and Padovani, 1995).

Previous studies have investigated the dynamics of the disc-corona system using the standard lamp-post geometry. The time delays caused by different photons travel times from the corona to the disc and observer (or "reverberation lags") can provide information about the disc-corona geometry. The majority of the previous research has focused on examining X-ray reverberation signatures in the lag-frequency spectra (Cackett et al., 2014; Emmanoulopoulos et al., 2014; Chainakun et al., 2016). Nevertheless, the study on X-ray variability power in AGNs utilizing the power spectral density (PSD) has shown that X-ray reverberation signatures are also detectable in PSD profiles (Papadakis et al., 2016; Chainakun, 2019). It is possible to determine the coronal height of AGNs from the reverberation signatures imprinted in the PSD profiles (Emmanoulopoulos et al., 2016; Chainakun et al., 2022;).

In a previous study (Chainakun et al., 2021), a support vector machine (SVM) machine learning model was used to classify the simulated Power Spectrum Density (PSD) of AGNs and predict the height and inclination angle of the corona. The SVM model was found to accurately extract these reverberation signatures from the PSD spectra and predict coronal height, but the model was tested only with simulated data. Additionally, the previous work focused on a "classification" problem; therefore, the prediction result from the SVM model was a "type" of data (e.g., the ML classifies PSDs as type 'A' which corresponds to the X-ray source height of 16-20 r_g). Note that $1r_g=1GM/c^2$, G is the gravitational constant, M is the mass of the supermassive black holes (SMBH), and c is the speed of light.

The classification algorithm is a predictive model that estimates and assigns labels or categories to discrete output variables based on input variables. It is not suitable for predicting continuous values or real values. On the other hand, the regression algorithm is specifically designed for predicting continuous values. It can better capture the inherent nature of the data to predict values that can reveal the true nature of the physical process.

Here, we use the regression algorithm, the random forest regression model, to predict the continuous values of the AGN physical parameters, e.g., coronal height, inclination, and black hole mass. Our ultimate goal is to use the regression model to investigate the variability occurring within the innermost regions of AGN IRAS 13224-3809 and 1H0707–495. Specifically, we aim to analyze the evolution of the corona in these AGN based on the archival XMM-Newton observations.
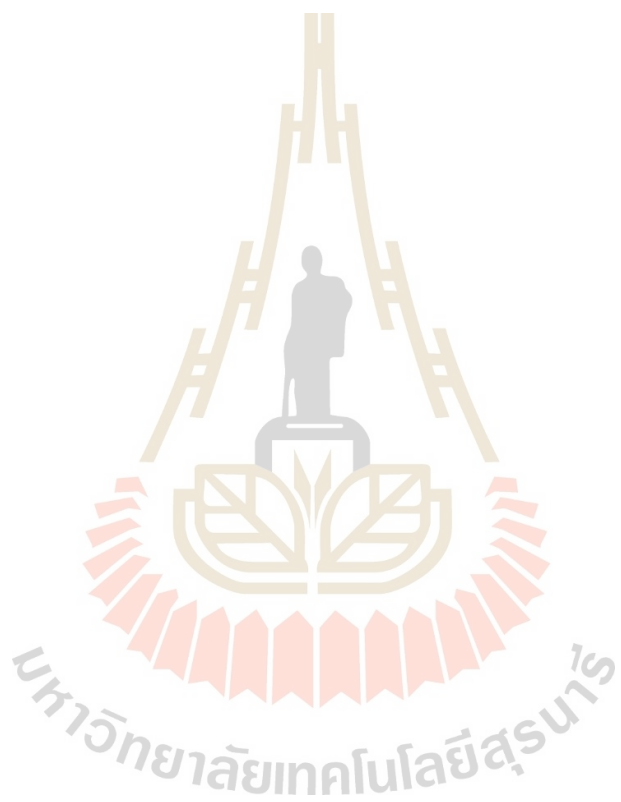
CHAPTER II

LITERATURE REVIEW

2.1 Active Galactic Nucleus (AGN) and reverberation signal.

The AGN is situated at the center of an active galaxy and emits a significant amount of X-ray radiation with high luminosity of $L=\sim10^{40}$erg/s. The AGN comprises of a central SMBH with the mass of 10^5 - $10^{10}M_\odot$, an accretion disc, and occasionally a relativistic jet (Curtis, 1918; Nowak and Wagoner, 1991; Fabian, 1999). The emissions from AGNs span a broad range from the radio to the hard X-ray bands. Numerous studies propose that the X-ray emissions originate from a region known as the "corona," although there is ongoing debate regarding its precise shape and location. Figure 2.1 illustrates some of the potential corona shapes that have been proposed.
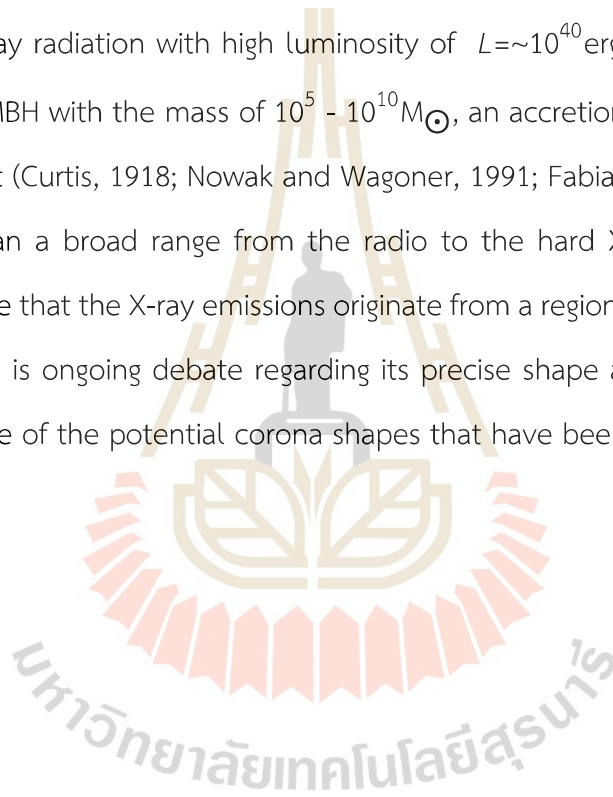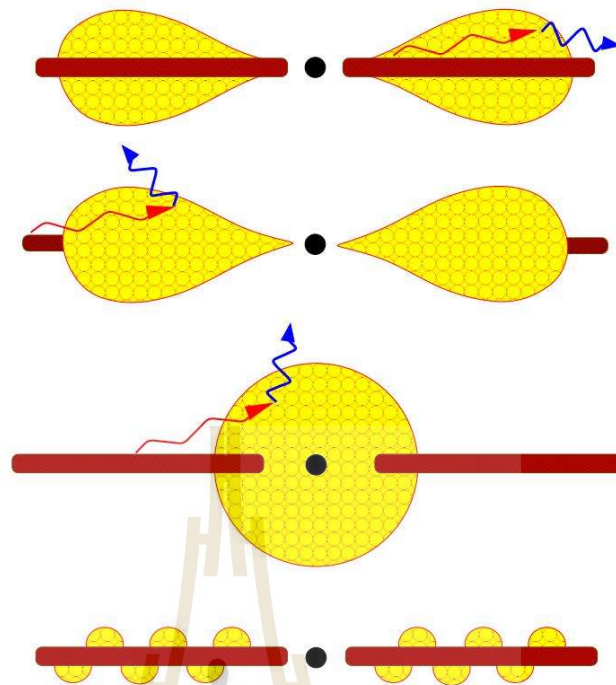
Figure 2.1 Suggested shape and geometries for the X-ray corona, where these is a black hole at the center surrounding by an accretion disc (red region). The yellow region is the X-ray corona (Reynolds and Nowak, 2003).

However, there is a simplified corona model called the "lamp-post model (LPM)" (Emmanoulopoulos et al., 2014; Uttley et al., 2014; Chainakun et al., 2016; Epitropakis et al., 2016; Papadakis et al., 2016) (see Figure 2.2). Typically, the LPM geometry assumes a point-like X-ray source situated on the rotational axis of the SMBH. On the other hand, an accretion disc is usually assumed to be optically thick and geometrically thin that extends from the innermost stable circular orbit (ISCO) to $\sim 1,000$ r_g (Emmanoulopoulos et al., 2014; Papadakis et al., 2016; Bambi, 2018; Caballero-García et al., 2020)

Basically, the corona produces the hard X-ray radiation (Haardt and Maraschi, 1991; Bambi, 2018). This occurred by inverse-Compton scattering of low-energy optical/UV photons from the disc (red line in Figure 2.2) by high-energy electrons within the corona, producing X-ray photons (blue line in Figure 2.2). The corona's X-ray

emission can be directly observed using the space X-ray telescopes such as XMM-Newton.

However, it is possible for the accretion disc to reflect primary X-ray radiation originating from the corona. This phenomenon produces another X-ray component referred to as "reflection" (green line in Figure 2.2). As the reflection photons travel a longer distance to the observer than the primary photons from the corona, they experience a time delay known as "reverberation lags." The light travel distance between the corona and the disc governs this delay, and measuring it enables us to determine the size and geometry of the system, e.g., the corona's location, inclination, and black hole mass (Cackett et al., 2014; Emmanoulopoulos et al., 2014; Uttley et al., 2014; Chainakun et al., 2016)
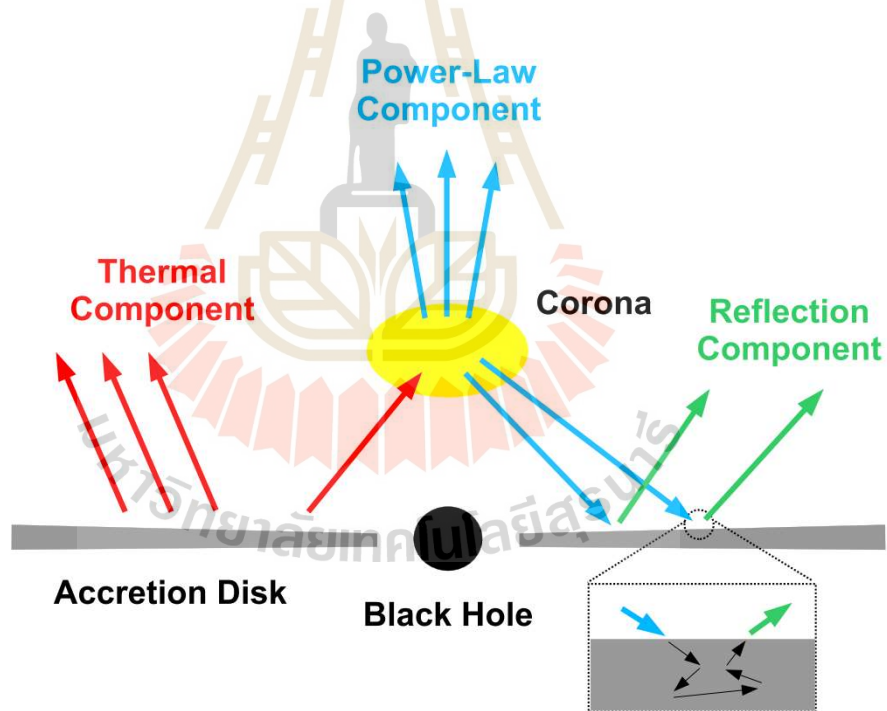
Figure 2.2 Disc-corona geometry of the lamp-post model (Bambi, 2018).

Nevertheless, observers can only detect a blend of signals between the primary and reflected X-rays and other component, as shown in Figure 2.3. To extract the time

delay for reverberation between these two X-ray components, timing techniques must be employed. One effective approach involves using response functions to analyze the reverberation lags, which will be explained in the next section.
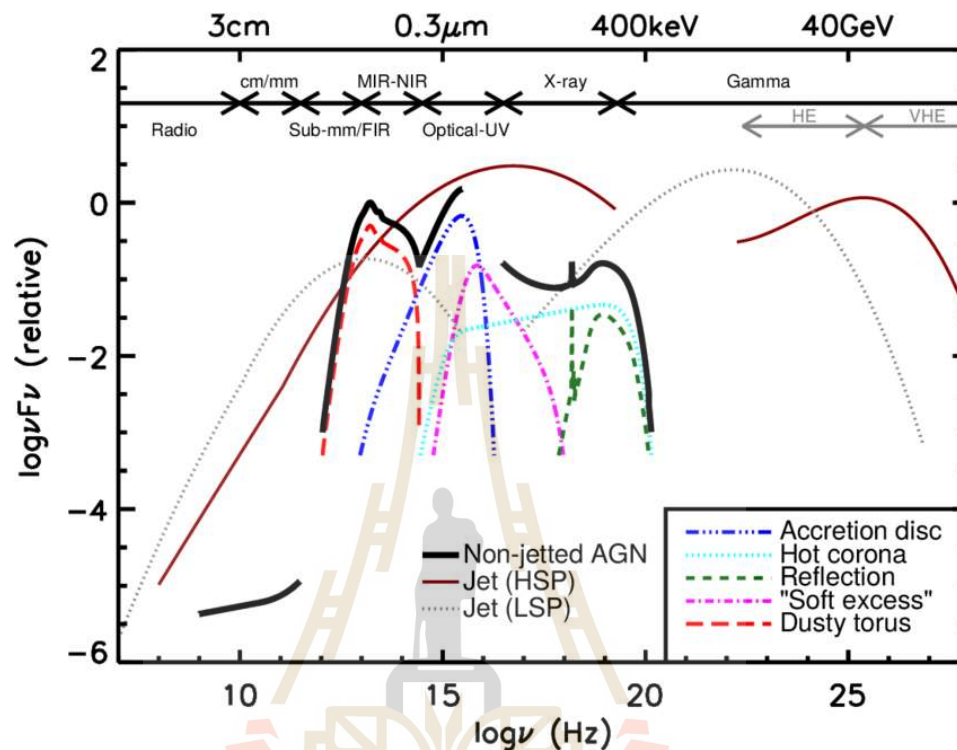
Figure 2.3 The AGN spectral energy distribution (SED) is constructed using the observed SEDs of non-jetted quasars. The solid black curve depicts the overall emission, while the different colored curves represent individual components. The blue line corresponds to the emitted accretion disc radiation, the light blue line represents emission originating from the corona, and the green line represents emission resulting from reflection on the disc. Additionally, the pink and red lines correspond to the soft excess phenomenon and torus emission surrounding the black hole, respectively (Padovani et al., 2017).

2.2 Reverberation feature

2.2.1 Response function of accretion disc

The response functions were widely applied to study X-ray reverberation time delays in both AGN and X-ray binaries (Emmanoulopoulos et al., 2014; Chainakun et al., 2019; Ingram et al., 2019). The response function of the disc can provide information of how photons from the corona are reflected off the disc. Figure 2.4 show an example of the response functions due to the X-ray reverberation around the black hole obtained from the relativistic ray-tracing simulations. These simulated response functions illustrate the echoes created by an instantaneous flash of the isotropic X-ray source when we vary three parameters including the black hole spin, inclination angle, and corona height. The x-axis represents the echo time delays of the photons reflecting from different parts of the accretion disc. The time zero indicates the point at which we begin to detect the direct photon from the corona. The reverberation response profile exhibits a rapid rise, following by two peaks and a decay, with the initial peak emerging from the first batch of photons that hit the near side of the accretion disc. But Some photons reflect with the inner region near the central black hole which has strong gravity, causing the function to become distorted and generating the second peak due to the intense gravitational field. The response function's decay results from photons colliding with the disc's outer region farther away from the central black hole. The flux is relatively weak and the response gradually fades away (Emmanoulopoulos et al., 2014).
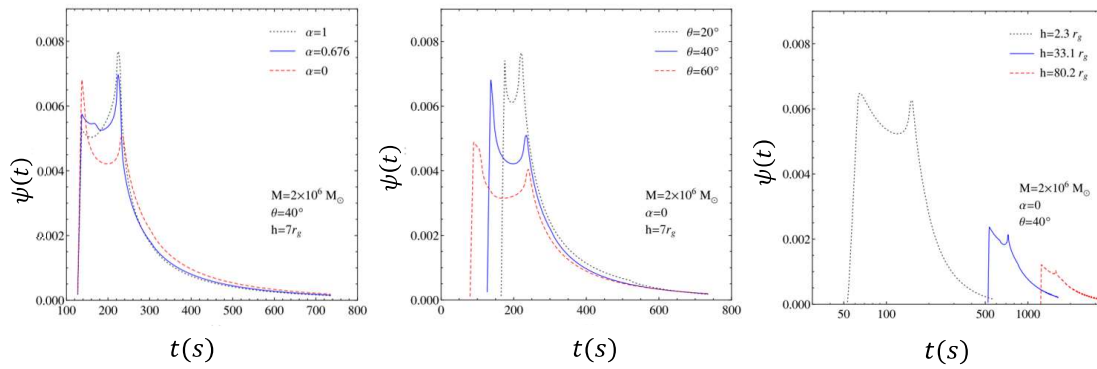
Figure 2.4 The impulse response of the X-ray reflection from an accretion disc. The left, middle and right panels show the cases when we vary the black hole spin, inclination angle and corona height, respectively (Emmanoulopoulos et al., 2014).

Figure 2.4 demonstrates that all of these parameters directly affect the response function. However, Reynolds, 2021 found that the majority of black holes exhibit a rapid spin, with $a > 0.9$, as shown in Figure 2.5. Consequently, for this study, we have chosen to keep the black hole spin parameter (a) fixed at 0.998 and allow the remaining parameter to vary.
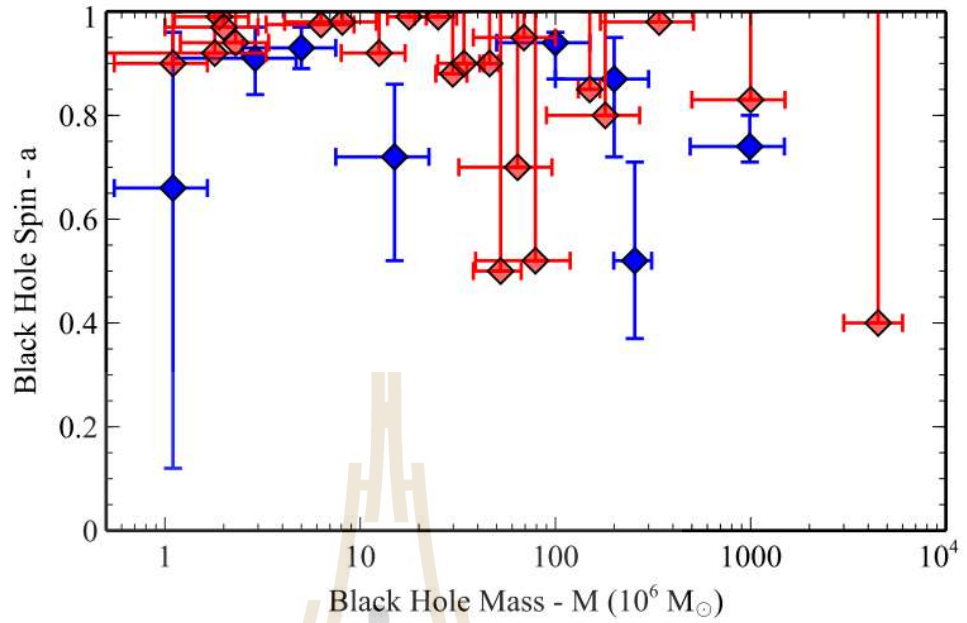
Figure 2.5 The relationship between the supermassive black hole mass and the spin in 34 AGNs. Lower limits show in the red line, and upper and lower measurements are in the blue line (Reynolds, 2021).

2.2.2 Reverberation feature imprinted on PSD profile

We used the convolution theory to simulate the PSD data imprinted with the reverberation features due to the lamp-post source. The convolution system is a mathematical operation that has two functions: one is a driving signal and the other is the response function. The driving signal is filtered by the response function to produce the third function, which is typically thought of as a modified form of the original driving signal (Atangana, 2018). The equation for the convolution written in the time domain can be expressed as

$$y(t) = \int_0^t h(\tau)u(t - \tau)d\tau = \int_0^t h(t - \tau)u(\tau)d\tau = u * h \, , \qquad [1]$$
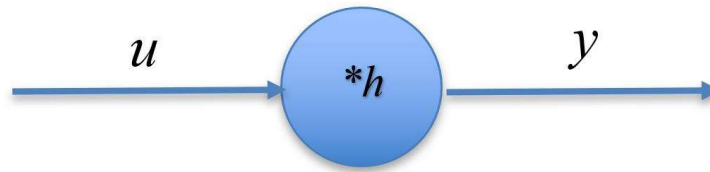
Figure 2.6 Block diagram of the convolution system in the time domain.

where u is the input function, h is the impulse response function, and y is the output signal (Figure 2.6).

In the frequency domain, the equation becomes

$$Y(f) = H(f)U(f) \, , \qquad [2]$$

Figure 2.7 Block diagram of the convolution system in the frequency domain.

where U is the input signals transformed into the Fourier frequency domain, H is the transfer function (response function in the frequency domain is usually called the transfer function), and Y is the output signal in the frequency domain. In our case, U is the X-ray variability power of the primary emission (or PSD), H is the Fourier form of the disc response function (referred to as the transfer function), and Y is the observed PSD representing the primary variability encoded with the response function (Figure 2.7).

After convolving the PSD with the transfer function due to X-ray reverberation, Papadakis et al. (2016) found that the characteristic features such as corona height, inclination angle, and black hole spin could be imprinted in the observed PSD profiles (Figure 2.8). These characteristics appear as an oscillatory structure, making them useful

for investigating the innermost region of AGN. As can be seen in Figure 2.8, both amplitude A_d and the frequency where the main dip appears are dependent strongly on the corona height. Note that amplitude A_d is the maximum amplitude of the first (main) dip. The A_d also increases significantly with increasing black hole spin. However, these amplitude and frequency are relatively less dependent on the inclination angles. The aim of this work is to develop the machine learning model that can extract these reverberation signatures on the PSD data of the AGN, and predict the coronal height which is the key parameter to study the coronal evolution in AGN.
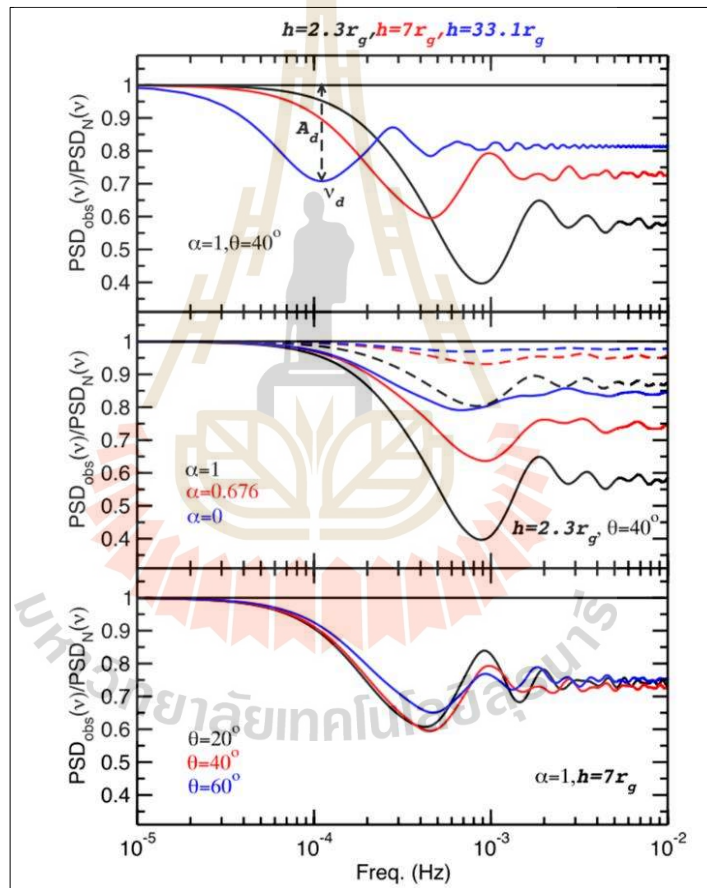
Figure 2.8 The PSD ratio that reveals X-ray reverberation features (Papadakis et al., 2016).

2.3 Corona evolution

Numerous studies have demonstrated that the X-ray corona is changing its location along the axis of the supermassive black hole. For instance, Alston et al. (2020) reported that the corona of the AGN IRAS 13224-3809 can vary its height between 6-20 r_g, as determined through lag-frequency spectra analysis. They also found the corona height tends to increase as the luminosity of the corona increases, as shown in Figure 2.9.
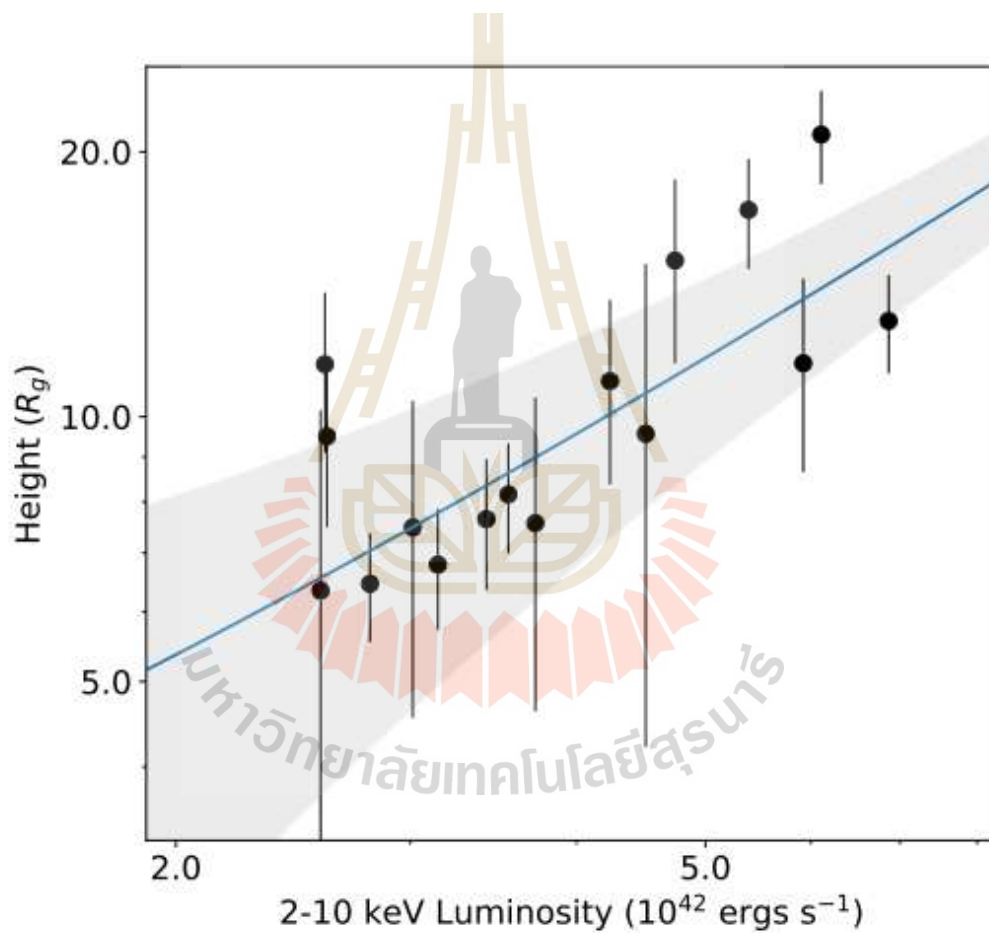
Figure 2.9 The relationship between the corona height and the observed 2-10 keV luminosity. The data and its 1σ error bars were used to create a weighted linear regression (Alston et al., 2020)

This finding was later supported by Caballero-Garcia et al. (2020), who reported a height variation of $3\text{-}10_{-3}^{+10}$ r_g. Similarly, by analysis PSD data of IRAS 13224-3809,

Chainakun et al. (2022) found that the corona can change its height between 3-25 r_g. This scenario recently found in NGC 5548 (Panagiotou et al., 2022).

2.4 Machine learning

In our previous study (Chainakun et al., 2021), we developed a machine learning model that used dictionary learning and support vector machine to predict the discrete values of coronal height and inclination angle from simulated PSD profiles. In this study, our goal is to predict the coronal height from real observational data, by using random forest regression to predict the continuous values of the coronal height

2.4.1 Random forest regression

We develop a ML model via the bootstrapping random forest (RFR) algorithm available in sci-kit learn (Pedregosa et al., 2011). The bootstrapping RF algorithm combines bootstrap aggregating and ensemble learning methods with multiple decision trees that have more power prediction than using just 1 decision tree.

A decision tree is a type of supervised learning algorithm employed for classification or regression tasks. It follows a hierarchical flowchart structure resembling a tree, where the root node initiates the process and subsequent nodes split the data based on specific parameters (decision nodes). This splitting continues until the leaf node is reached, providing a final result that meets the desired criteria (Figure 2.10).
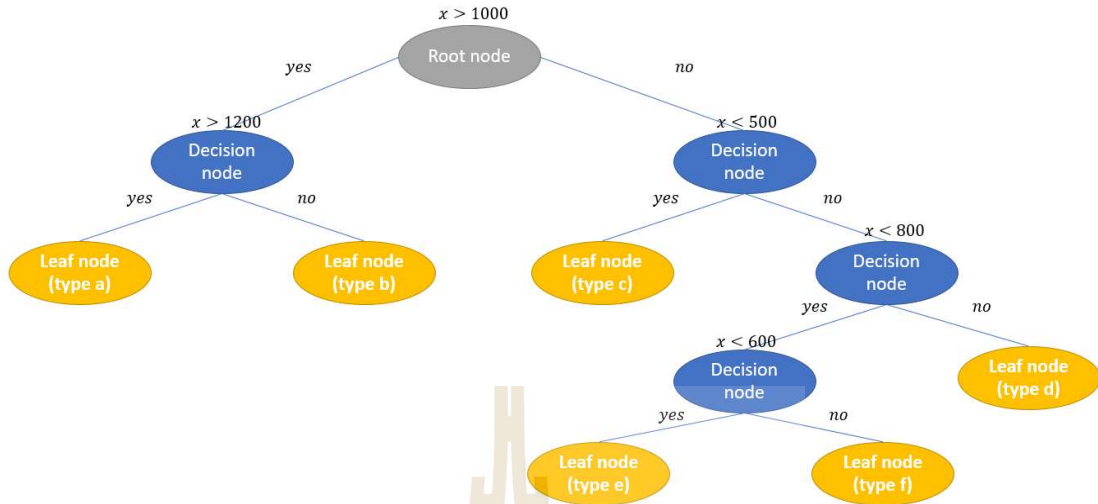
Figure 2.10 Decision tree diagram.

Let us assume the training set X=($[x_1]...,[x_n]$) with responses (i.e., things we want to predict) Y = ($y_1...,y_n$), where n is the total number of the samples. Each sample $[x_i]$ can contain several features. The length (dimension) of $[x_i]$ represents a total number of features which in our case, are the variability power in each Fourier frequency bin. For example, if we have 100 PSD samples and we bin each PSD data into 20 bins, then n = 100 and the number of the features for each $[x_i]$ sample is 20.

The RFR algorithm used here is summarized as a flowchart in Figure 2.11. During the bootstrapping process, 60% of the training set is selected by randomly sampling with replacement with a number of features about ~1/3. This process is repeated T time meaning that we have T decision trees ($t=1...,T$) in the forest. For each regression tree, new training set D_t with responses Y_t is produced, and trained and tested via the model given by f_t. The ensemble learning is initiated by using f_t to predict the unseen data set X'. Then, the result is from averaging all individual predictions on the unseen samples X' from all individual regression trees (Breiman, 1996, 2001). This leads to a model that can be written as

$$\hat{f} = \frac{1}{T}\sum_{t=1}^{T} f_t(X') ,$$

[3]
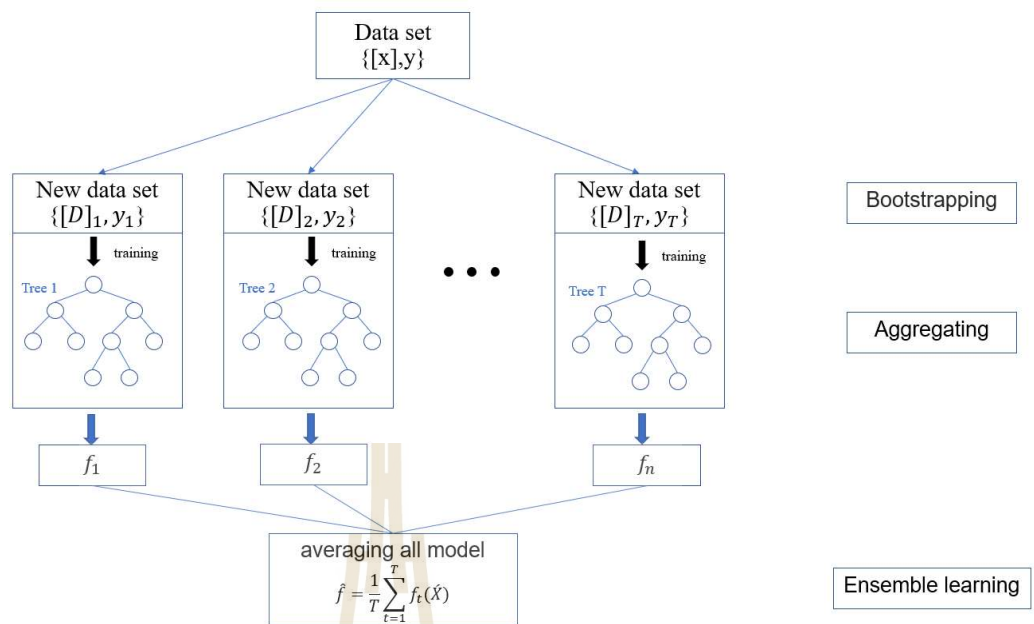
Figure 2.11 Flowchart showing the structure of the random forest bootstrap process.

CHAPTER III

METHODOLOGY

3.1 Observational data

This work considers two AGNs including IRAS 13224-3809 and 1H 0707−495, which are high variability source (Alston et al., 2018; Xu et al., 2021). There have been many X-ray observational data since 2000 that are suitable to use to probe the evolution of X-ray corona in these AGNs. All observational data were obtained from the XMM-Newton telescope as shown in Table 3.1.

Table 3.1 Observational data of AGNs IRAS 13224-3809 and 1H 0707−495 since 2000. The first, second, third, fourth, and fifth column represent the observation ID, revolution number, date for each observation, exposure time to detect the photon and count of photon that detected.

Observation ID	Revolution number	Observation -al date	Exposure time (ks)	Count rate (count s^{-1})
IRAS 13224-3809				
0673580101	2126	2011-07-19	34.08	0.37
0673580201	2127	2011-07-21	49.26	0.24
0673580301	2129	2011-07-25	52.03	0.09
0673580401	2131	2011-07-29	85.11	0.28
0780560101	3037	2016-07-08	39.38	0.19
0780561301	3038	2016-07-10	112.35	0.26
0780561401	3039	2016-07-12	99.76	0.22

Table 3.1 (Continued).

Observation ID	Revolution number	Observation--al date	Exposure time (ks)	Count rate (count s^{-1})
0780561601	3044	2016-07-22	97.85	0.38
0780561701	3045	2016-07-24	100.13	0.16
0792180101	3046	2016-07-26	110.64	0.13
0792180201	3048	2016-07-30	110.55	0.19
0792180301	3049	2016-08-01	86.44	0.07
0792180401	3050	2016-08-03	98.63	0.75
0792180501	3052	2016-08-07	102.66	0.23
0792180601	3053	2016-08-09	101.50	0.68
1H 0707-495				
110890201	159	2000-10-21	29.94	0.13
148010301	521	2002-10-13	57.98	0.66
506200301	1360	2007-05-14	33.38	0.25
506200501	1379	2007-06-20	20.52	1.03
511580101	1491	2008-01-29	68.69	0.60
511580201	1492	2008-01-31	43.88	1.01
511580301	1493	2008-02-02	37.39	0.66
511580401	1494	2008-02-04	50.62	0.56
653510301	1971	2010-09-13	93.30	0.53
653510401	1972	2010-09-15	78.46	0.80
653510501	1973	2010-09-17	81.51	0.49
653510601	1974	2010-09-19	79.65	0.57
554710801	2032	2011-01-12	48.54	0.04

3.2 PSD simulation

We use the kynxilrev model (Caballero-García et al., 2020) to compute the disc-response functions (φ) under the lamp-post hypothesis with a fixed black hole mass of $10^6 M_\odot$ and the black hole spin of a =0.998. the source height is varied to be 2.3, 4, 6, 8, 10, 12, 14, 16, 18, 20, 22, 24, 26, 28, 30 r_g. Basically, the kynxilrev is the realistic ray-tracing simulation to trace the trajectories of the photons between the corona, the accretion disc, and the observer, by assuming a point-like X-ray source.

Once the response function (φ) is obtained, the total response function can be written as

$$\Psi(t) = \delta(t) + R\varphi(t) \, , \qquad [4]$$

where $\delta(t)$ is a delta function for the primary radiation, $\varphi(t)$ is the disc response function, and R is a normalization factor representing the reflection fraction (R_f) defined as the ratio of (reflection flux / continuum flux).

The AGN viability power can be measured via the power spectral density (PSD) that, motivated by observations, can be written in a simple form of a power law:

$$P(f) \propto f^{-\Gamma} \, , \qquad [5]$$

where f is the Fourier frequency, and Γ is the power index.

Therefore, the observed PSD taken into account the X-ray reverberation effects can be obtained by (Uttley et al., 2014; Chainakun et al., 2021; Chainakun et al., 2022) :

$$P_{obs}(f) = |\Psi(f)|^2 P(f) \, , \qquad [6]$$

where $P_{obs}(f)$ is the PSD of the AGN that included the reverberation effects and $\Psi(f)$ is the total response function that is already transformed to be in the Fourier frequency domain. Note that we train the machine using $P_{obs}(f)$ in order to

predict the source height and the inclination. The number of features is then the number of bins used to generate $P_{obs}(f)$.

Here, we simulated PSD to investigate potential of RFR model in 2 cases :

- Case I : General RFR model for predicting the coronal height and inclination : we simulated the response functions by varying the source height between 2.3-30 (n=15) with the inclinations of 5, 30 ,45, 60, and 75 degrees (n=5). These response functions are convolved with the simple form of a power law (eq.5) with the varying power index between 1.6-3.5 (n=20) and fixed the reflection fraction to be 1. Therefore, there are 1500 samples of the observed PSD where the reverberation features are imprinted into (-eq. 6-). The noise is then added in the PSD following Timmer and Koenig, 1995.

- Case II : The RFR model to probe real observational data of IRAS 13224-3809 and 1H 0707–495 : we simulated PSD as same as previous cases, but we fixed the inclinations angle to be 45 degree and varied the reflection fraction between 0.6-1.6 (n=6). Therefore, in this case, we have 1800 samples of the observed PSD. Then, we modify the PSD's frequency bin appropriate to individual observations.

3.3 Machine leaning process

The RFR model is developed using sklearn.ensemble.RandomForestRegressor available in sci-kit learn (Pedregosa et al., 2011). There are many hyperparameters that could be tuned to increase the prediction accuracy, for example.

- n_estimators: Number of decision trees in the RFR model.
- max_features: Maximum number of features that the RFR model considers to split a node.
- max_depth: The maximum depth of individual tree
- mini_sample_leaf: The minimum number of leaves required to split a decision node.
- criterion: Function to split the node.
- max_leaf_nodes: Maximum leaf nodes of individual tree

However, two key hyperparameters that have a powerful effect on prediction performance are n_estimators and max_depth. Therefore, we select to fine-tune only n_estimators and max_depth. Other parameters are set to default. To investigate the potential of the RFR algorithm, we split 1500 (Case I) or 1800 (Case II) samples of our prepared PSD into 80% for the training set and 20% for the testing set.

To optimize the performance of the RFR model, we used a method called GridSearchCV in scikit-learn. This method involves tuning the hyperparameters of the model by performing a K-fold cross-validation process, where the training set is further divided into K folds. Here, we set K=5. For each iteration, the model is trained on 4 of the folds and validated on the remaining fold. This process is repeated 5 times, with each fold being used for validation once.

During this process, the hyperparameters of the model are systematically varied over a range of values, and the best combination of hyperparameters is determined based on the coefficient of determination, denoted as R^2 score. This coefficient measures how well the model fits the data, with a maximum value of 1 indicative of a perfect fit with actual results while 0 indicates no correlation between the predicted

and actual results. The hyperparameters that produce the highest R^2 score are chosen as the optimal values for the model.

Finally, the RFR model is modified further for the specific case of the AGN IRAS 13224-3809 and 1H 0707–495. The mass, inclination, as well as the number of the frequency bins used to extract the PSD are fixed to those values comparable to what reported in previous studies (e.g. Zhou and Wang, 2005; Alston et al., 2020; Chainakun et al., 2022).

CHAPTER IV
RESULT

4.1 General RF model for predicting the coronal height and inclination (Case I)

Figure 4.1 displays an example of the simulated PSD profile in the form of a simple power-law imprinted with X-ray reverberation feature. By following the process outlined in CHAPTER III, we first obtained the initial clean PSD (top panel in Figure 4.1) that exhibits characteristic reverberation features, manifesting as oscillatory patterns such as dips and bumps within the frequency range of 10^{-3}-10^{-2}Hz. For this process, we employed 256 frequency bins. Subsequently, we introduced noise to the PSD following the method of Timmer and Koenig (1995). It is important to emphasize that we utilized the PSDs that include noise (bottom panel in Figure 4.1) to train the machine learning model as they accurately represent the observations encountered in real-world scenario
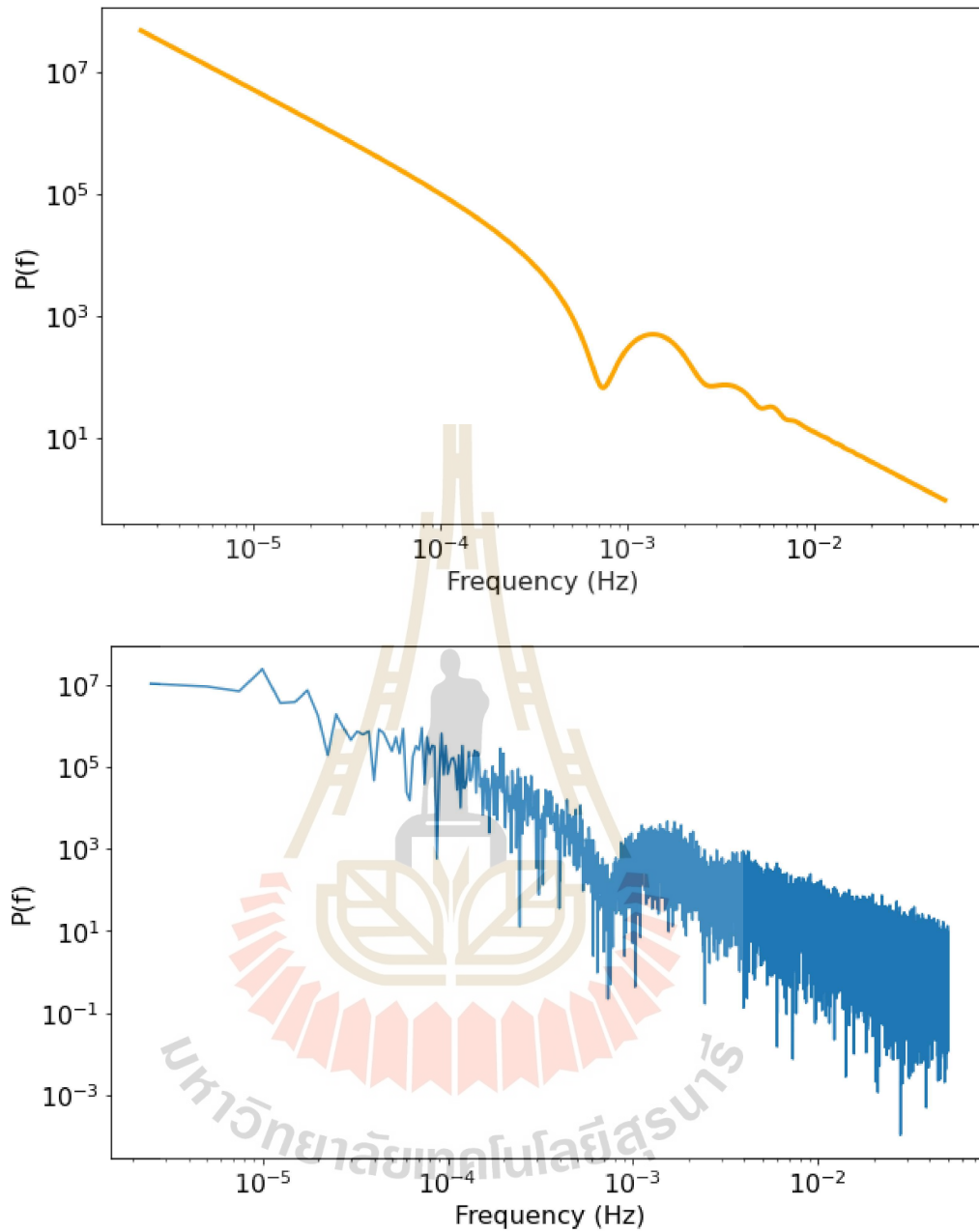
Figure 4.1 Example of the simulated PSD profile. Top panel is the clean PSD without noise and bottom panel is the PSD with noise generated using the method outlined by Timmer and Koenig (1995).

Figures 4.2 and 4.3 show the examples of the PSDs profile when we vary corona height and inclination angle. The effect of varying height and inclination are consistent with those in Papadakis et al. (2016) . We see the main dip move to higher Fourier-

frequency (shorter timescales) for lower height. Also, we can see that the inclination has relatively small effect on the profiles.
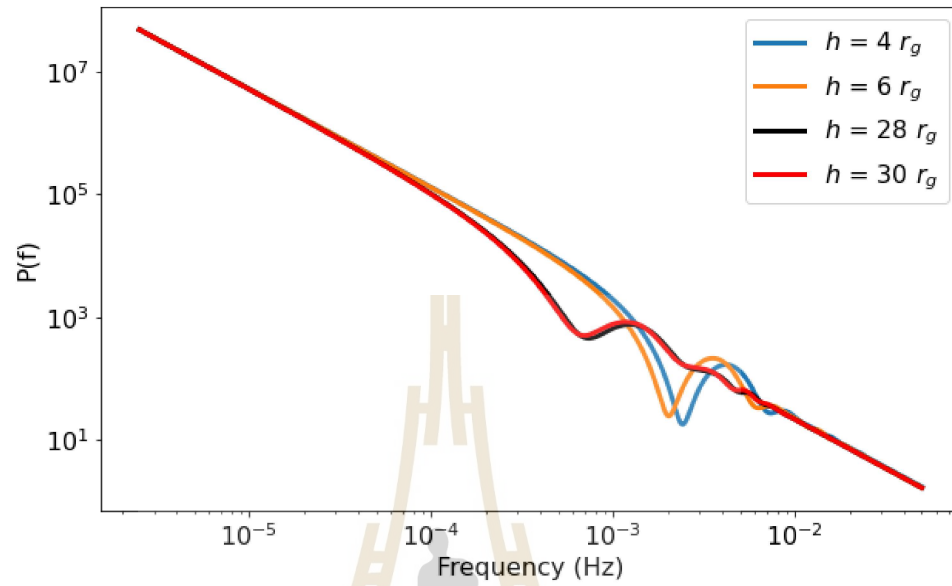
Figure 4.2 The PSDs profiles with the corona height of 4 r_g, 6 r_g, 28 r_g and 30 r_g. The inclination angle is 45°.
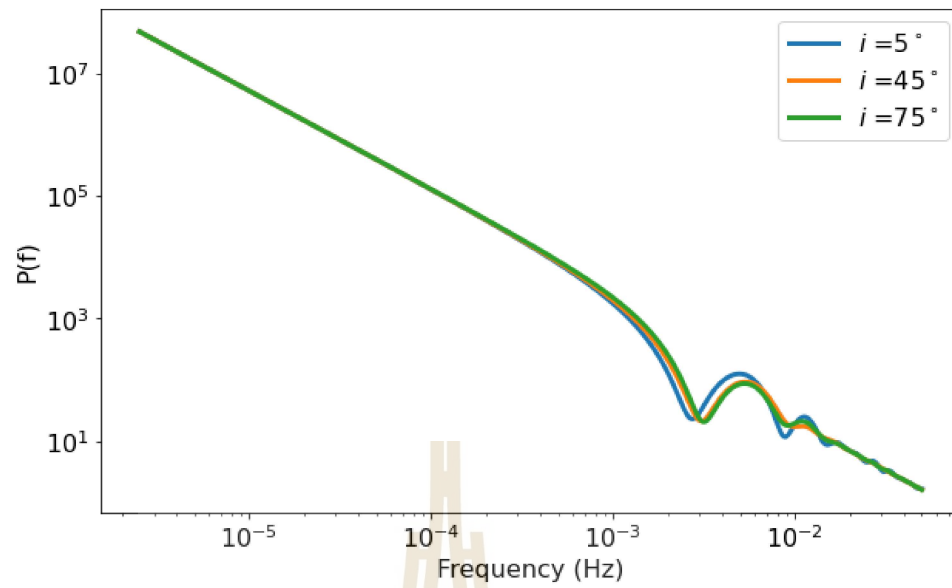
Figure 4.3 The PSDs with the inclination angle of 5°, 45° and 75°. The corona height is fixed at 10 r_g.

Figure 4.4 shows examples of the PSDs when the reflection fraction is varied. When the reflection fraction increases, the reverberation feature (the dip) is more prominent. This is resonable since higher reflection fraction means that the reverbaration signal is stronger.
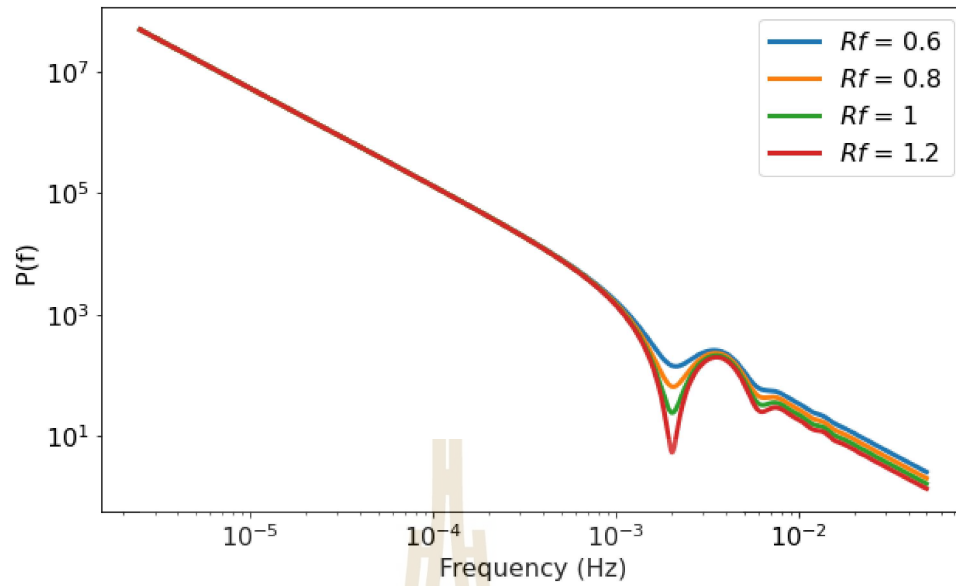
Figure 4.4 The PSDs when the reflection fraction is 0.6, 0.8, 1 and 1.2 . The inclination angle is 45° and the corona height is fixed at 4 r_g.

Figure 4.5 shows the accuracy scores (expressed as R^2 values) obtained through the 5-fold cross-validation process. Note that the simulated PSD data consists of 1,500 samples (Case I). When predicting the coronal height solely, the maximum achieved R^2 is ~ 0.93, indicating the model has high accuracy compared to the case where only inclination angle is predicted. However, when attempting to simultaneously predict both the height and inclination, the maximum R^2 score drops to around 0.60. This suggests that predicting inclination is challenging due to the fact that different inclinations yield only subtle variations in the reverberation features presenting in the PSD profiles (see also Figure 4.3). Consequently, the decision has been made to focus exclusively on predicting the coronal height.
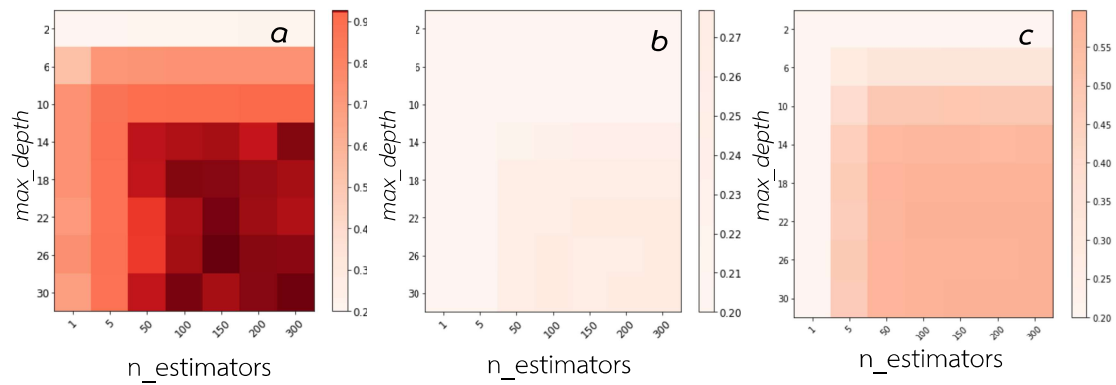
Figure 4.5 Heat map showing the obtained accuracy scores during the cross-validation process when a) predicting only the coronal height, b) predicting only the inclination, and c) predicting both height and inclination simultaneously.

Figure 4.6 shows the scatter plot between the true height and predicted height in the case of predicting only the coronal height. There is a good prediction at ~ 2.3-23 r_g and a poor prediction at very high source height because at the high source height the reverberation features on the PSDs are less significant (see Figure 4.2).
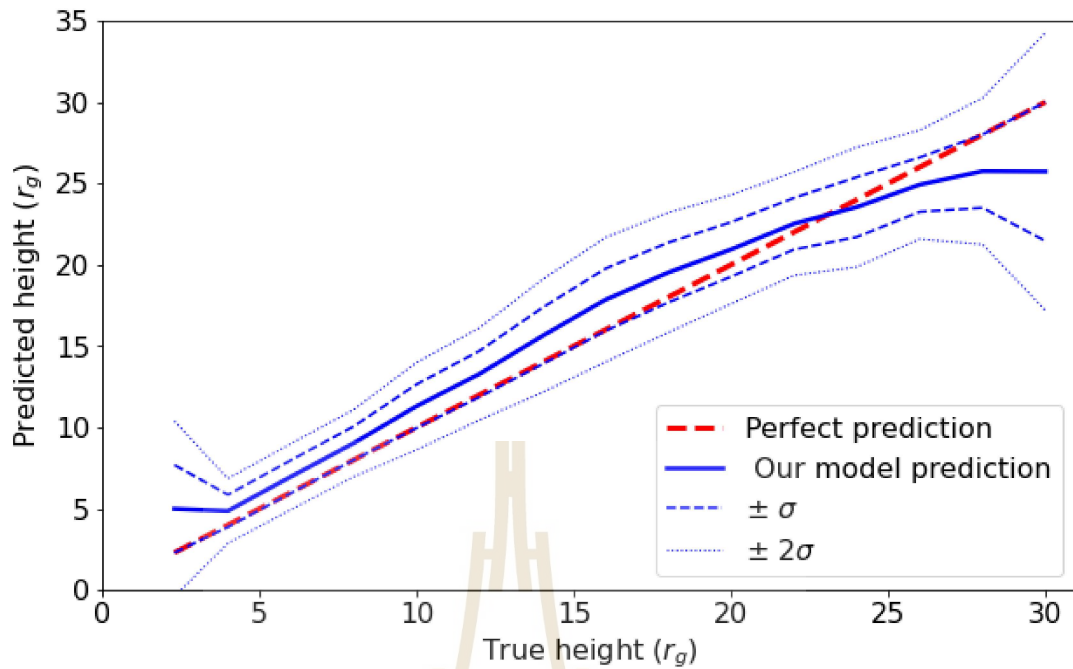
Figure 4.6 Scatter plot between the true height and predicted height. The RFR model's forecast is represented by the blue line while the ideal forecast line is shown by the red dashed line. The blue-dashed and blue-dotted lines indicate the areas where the predicted heights differ within ±1σ and ±2σ, respectively. Where the **σ** is standard deviation of prediction.

4.2 The RFR model to probe the corona evolution in the AGN IRAS 13224-3809 and 1H 0707–495 (Case II)

The RFR model is now being utilized to extract the reverberation features in the PSD data of IRAS 13224-3809 and 1H 0707–495. Initial investigations are conducted to determine the appropriate frequency range and bin sizes for the PSD, taking into account the length of each observation for IRAS 13224-3809 and 1H 0707–495.

We generate the modeled PSD data incorporating the reverberation effects, following a similar approach as before. However, for IRAS 13224-3809, we adjust the black hole mass to be $2\times10^6 M_\odot$ and fix the inclination at 45° (Alston et al., 2020; Chainakun et al., 2022). Similarly, for 1H 0707–495, the black hole mass is changed to $2.3\times10^6 M_{sun}$ and the inclination is fixed at 45° (Zhou and Wang, 2005). In this case, we vary the reflection fraction between 0.6 and 1.6.

The PSD profiles are then binned into ~30 Fourier-frequency bins, covering the frequency range of 10^{-5}- 2×10^{-3}Hz, which is consistent with what is typically observed in real data (see Figure 4.7). Note that in this case the number of frequency bins is significantly lower than what used in Case I (Section 4.1)
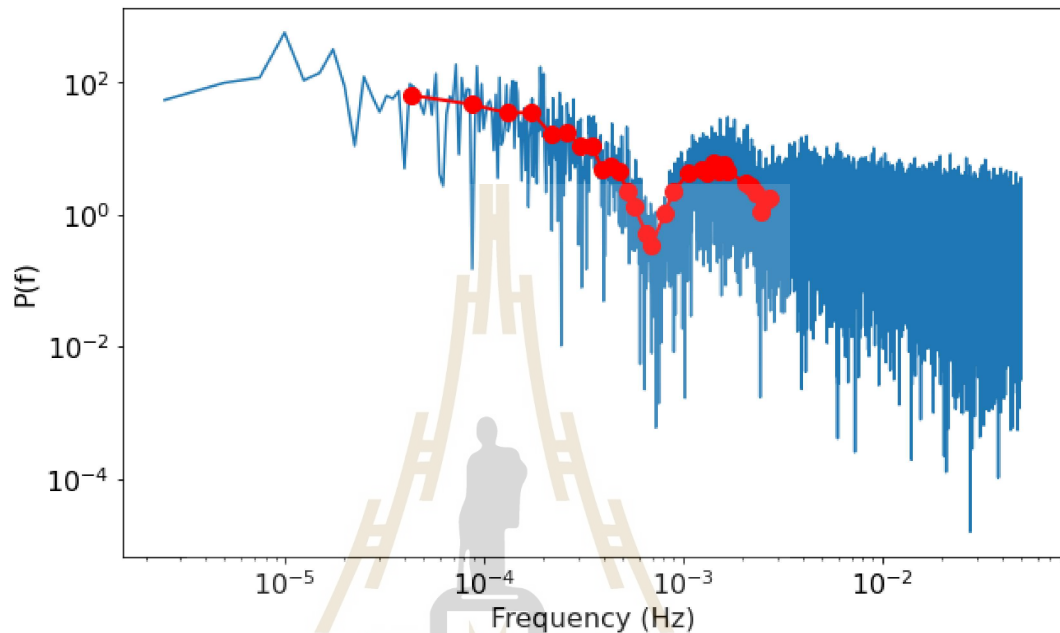
Figure 4.7 PSD profiles binned into ~30 frequency bins shown in the red dotted line, corresponding to what can be probed in IRAS 13224-3809 and 1H 0707–495, and the blue line is a simulated PSD profile before binned. The binned PSDs then are used to train the machine (Mankatwit et al., 2023).

Subsequently, we proceeded to train a random forest regression model using the binned PSDs. Figure 4.8 showcases the accuracy results obtained from fine-tuning the hyperparameters through 5-fold cross-validation. In this case, the maximum achieved accuracy R^2~ 0.95. The optimal hyperparameters are the maximum depth, and the number of estimators, which are approximately 26 and 200, respectively.
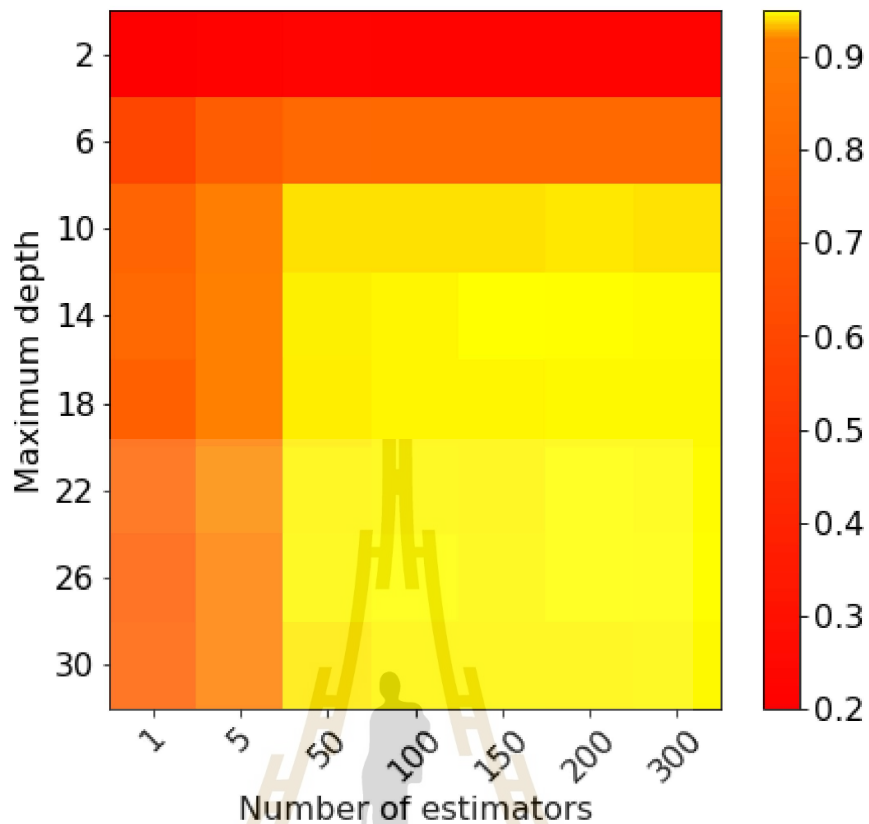
Figure 4.8 Obtained accuracy scores when the machine is trained using the binned PSDs. The AGN parameters as well as the number of frequency bins are set according to what is observed in IRAS 13224-3809 and 1H 0707–495. The model can still provide an accurate prediction of the coronal height, with $R^2 \sim 0.95$ (Mankatwit et al., 2023).

Figure 4.9 displays the true versus predicted values of the coronal height obtained using this random forest regression model. It is evident that the model can still provide accurate predictions of the coronal height even when the PSD data is binned into approximately 30 frequency bins. However, there is a low prediction accuracy observed at the heights of $\sim 2.3\ r_g$. This discrepancy arises because the reverberation feature imprinted in the PSDs lies outside the frequency range considered here (i.e., exceeding 2×10^{-3} Hz).
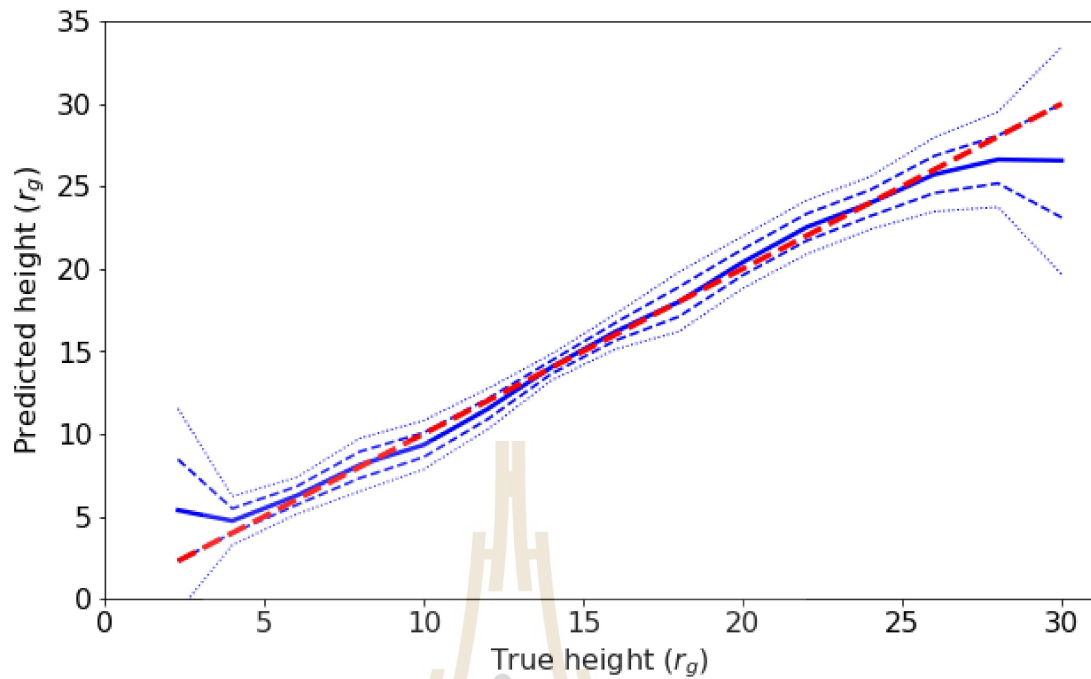
Figure 4.9 Scatter plot between the true and predicted height in the case of the binned PSDs. The AGN parameters as well as the number of frequency bins are set according to what is observed for IRAS 13224-3809 and 1H 0707−495. The model can still provide an accurate prediction of the coronal height, with $R^2 \sim 0.95$ (Mankatwit et al., 2023).

Figure 4.10 shows that the RFR model is more effective when the reflection fraction $R_f \geq 1$. This is because the reverberation are more prominent for higher R_f (see Figure 4.4), which means that the model is best to use with PSDs in the soft energy band such as in 0.3 - 1 keV where the reflection flux dominates.
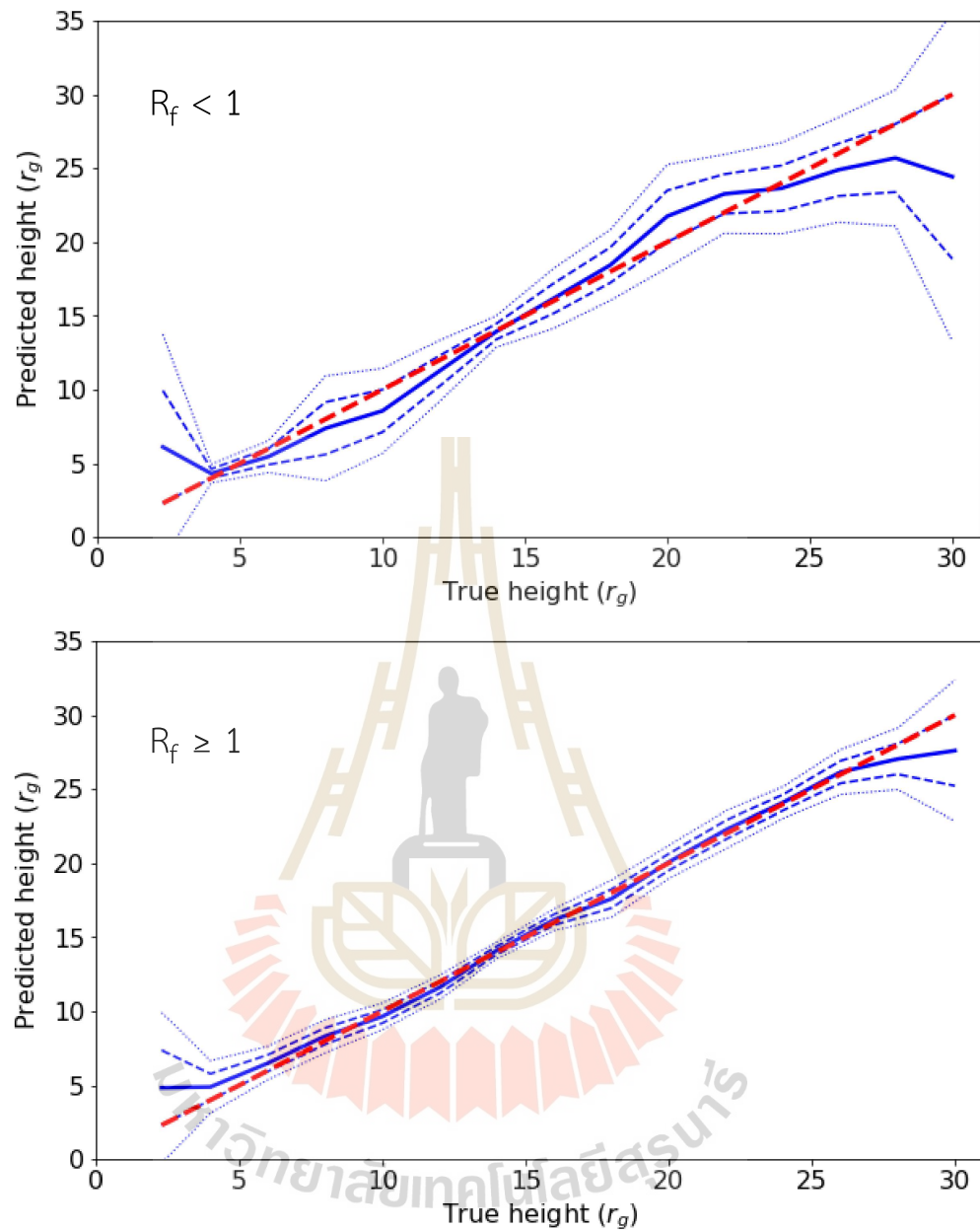
Figure 4.10 Scatter plot between the true height and the predicted height. Top panel presents the prediction of PSDs when the reflection fraction < 1 and bottom panel presents the prediction of PSDs when the reflection fraction ≥ 1 (Mankatwit et al., 2023).

The prediction accuracy when removing some frequency bins randomly is shown in Figure 4.11. This is relevant because in real observational data, certain bins may be dominated by Poisson noise. Our result shows that even with the removal of these frequency bins up to ~10 bin, the accuracy of the model is still high, with R^2 value greater than 0.9.
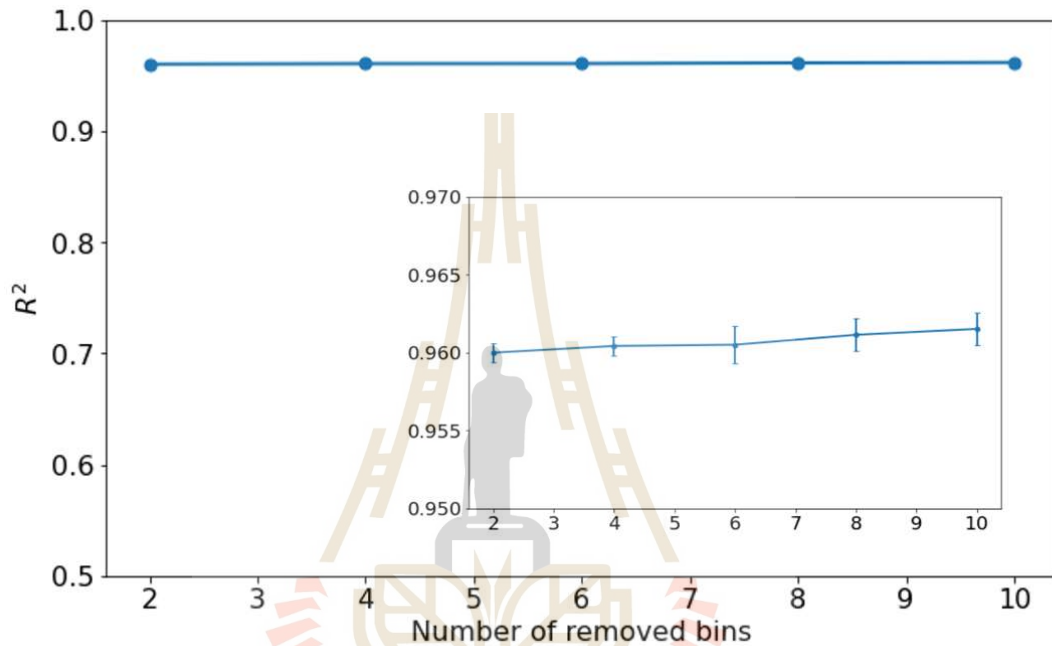
Figure 4.11 The prediction accuracy when we fixed the number of the frequency bins to be 30 and then randomly removed them out ~2-10 bins, the small figure shows the accuracy has a small variability when removing the frequency bins (Mankatwit et al., 2023).

Figure 4.12 shows how the accuracy of the model changes as the mass of the AGN being studied deviates from the value used to train the model. As the difference in mass increases, the accuracy of the model decreases. However, the results show that an R^2 value of approximately 0.9 can still be achieved even if the true mass is within a range of ±10% from the mass used to train the model.
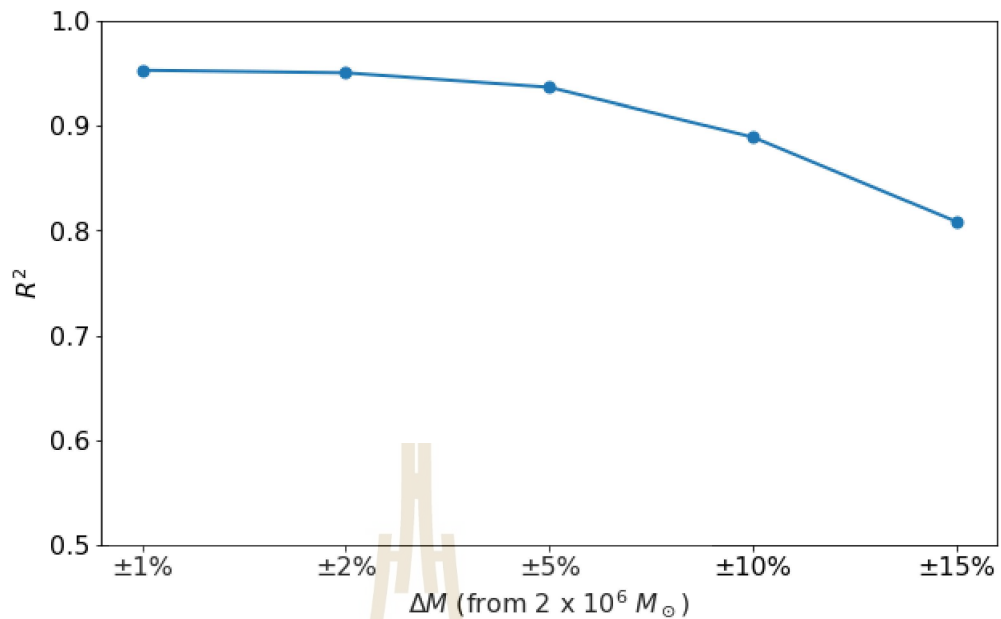
Figure 4.12 The accuracy of prediction when we test with variation black hole mass ~1-15% (Mankatwit et al., 2023).

The RFR model's prediction of the corona height compared to the count rates for IRAS 13224-3809 and 1H 0707−495 using the PSDs in 0.3−1 keV band is shown in Figure 4.13. Based on the analysis of 16 observations for IRAS 13224-3809 and 13 observations for 1H 0707−495, we find a moderate monotonic correlation between the coronal height and count rate. We conducted two tests, Test A and Test B, where we examined 20 PSD indices in the range of 0.5 to 2 and 40 PSD indices in the wider range of 0.5 to 4, respectively. The predicted corona heights differ slightly depending on the assumed power law PSD index range. However, the trend of an increasing source height with the count rate remains unchanged. In the case of IRAS 13224-3809, we find the Spearman correlation coefficient is 0.55 with the p-value of 0.029 for test A and Spearman correlation coefficient is 0.54 with the p-value of 0.032 for test B. In the case of 1H 0707−495, we find the Spearman correlation coefficient is 0.50 with the p-value of 0.082 for test A and Spearman correlation coefficient is 0.56 with the p-value of 0.047 for test B.
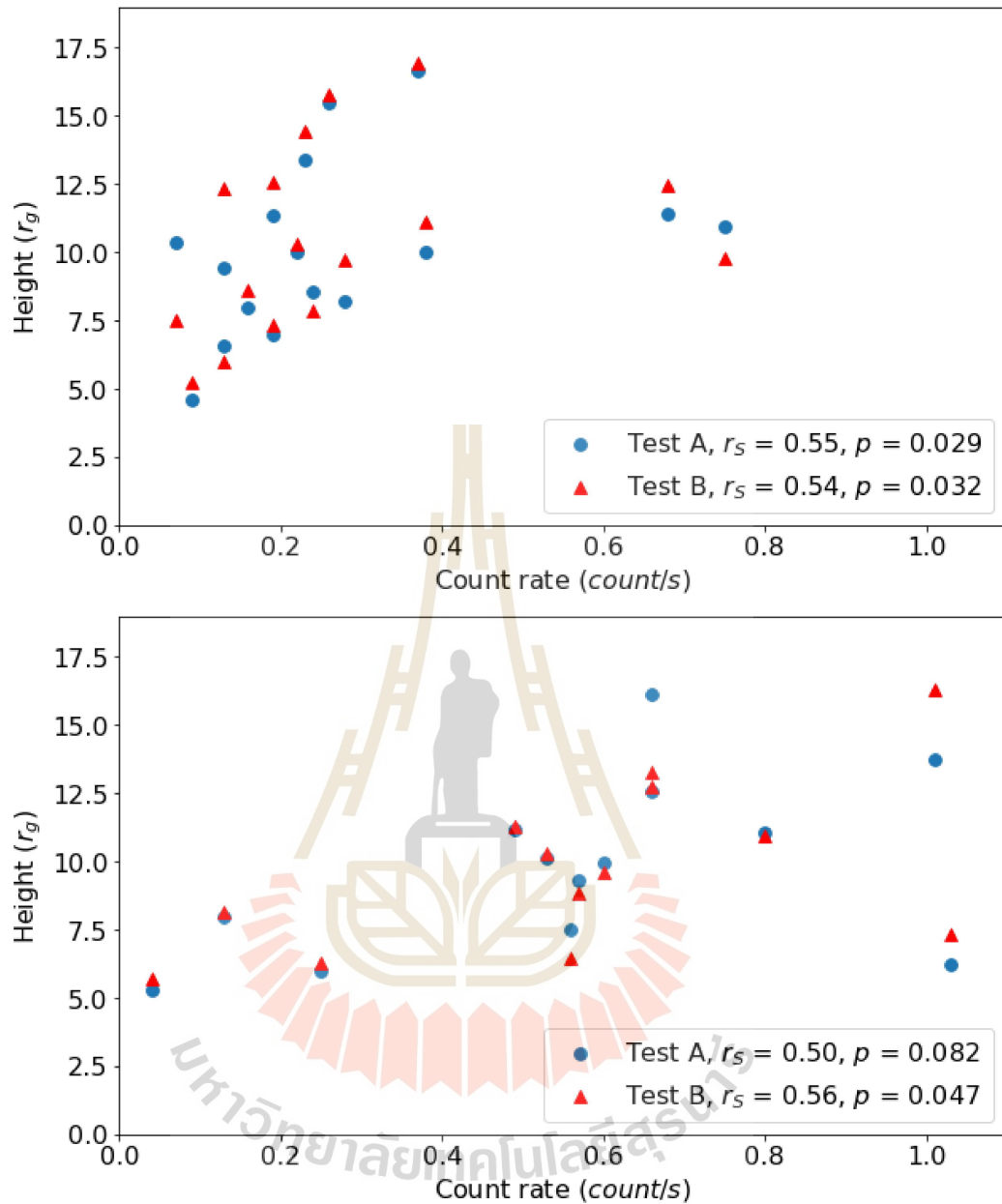
Figure 4.13 Coronal height versus count rate of the observations of IRAS 13224−3809 (top panel) and 1H 0707−495 (bottom panel) as predicted by the RFR models. Additionally, the Spearman correlation coefficient (r_s) and p-value (p) of this correlation are also provided (Mankatwit et al., 2023).

CHAPTER V

DISCUSSION AND CONCLUSION

Our research shows that machine learning techniques can potentially be used to study the coronal evolution in AGN. We have developed a random forest regressor model to predict the coronal height, black hole mass, or inclination angle using simulated PSD data sets and have applied it to real observed data. However, the accuracy of the model is limited when determining the inclination or black hole mass due to various factors. For example, the reverberation features may be unclear and difficult to extract (see Figure 4.2 and 4.3), or the model may require a larger number of PSDs with varying inclination angles to be trained. Additionally, the characteristics of PSDs that vary with mass can be similar to those that change with the source height (Papadakis et al., 2016).

We found that the coronal evolution in IRAS 13224-3809 and 1H 0707-495 can be estimated to be around 5-18 r_g. The significant moderate monotonic correlation between corona height and luminosity are revealed, with p-value < 0.05 (see. Figure 4.13). This finding supports the light-bending scenario (Miniutti and Fabian, 2004), where the corona moves closer or farther away from the black hole due to the fluctuations in the gravitational and magnetic fields caused by the interaction between the black hole and the accretion disc.

Our results are comparable with previous studies, particularly in AGN IRAS 13224–3809. Alston et al. (2020) used lag-frequency spectra and found a constrained coronal height of approximately 6-20 r_g. Caballero-García et al., 2020 used a combined spectral-timing analysis and found that the coronal height varies between approximately 3-10$^{+10}_{-3}$ r_g, assuming a maximally spinning black hole. More recently, Chainakun et al., 2022 traced the corona evolution from reverberation signatures

appearing in PSDs of IRAS 13224–3809 using conventional fitting techniques and found a varying corona located at the height of ~3-25 r_g.

Finally, our results suggest that machine learning techniques could potentially be used to investigate AGN variability in a range of other contexts. For example, future studies could use similar models to predict other properties of AGNs. We hope our project will inspire further research in this area and contribute to a better understanding of these fascinating astronomical objects. Nevertheless, machine learning techniques may also have an 'overconfident' problem. They make predictions for every input data regardless of whether it is relevant to the training set. In our case, machine learning predicts the height of every PSD without considering if the PSD characteristics are suitable enough to predict. For instance, it tries to predict the height of PSDs within the range of 2-5 r_g or 25-30 r_g without considering the prediction's uncertainty or high variance (see Figure 4.6 and Figure 4.9). There are some suggestions for solving this problem using deep learning, e.g., Bayesian neural network (see. Jospin et al., 2022). Furthermore, the frequency range dominated by Poisson noise does not appear randomly but rather arises due to the limitations imposed by the device. By identifying the specific frequency range in which Poisson noise is likely to occur, developing a machine learning algorithm that excludes this range from consideration becomes feasible, enhancing accuracy even further.

REFERENCES
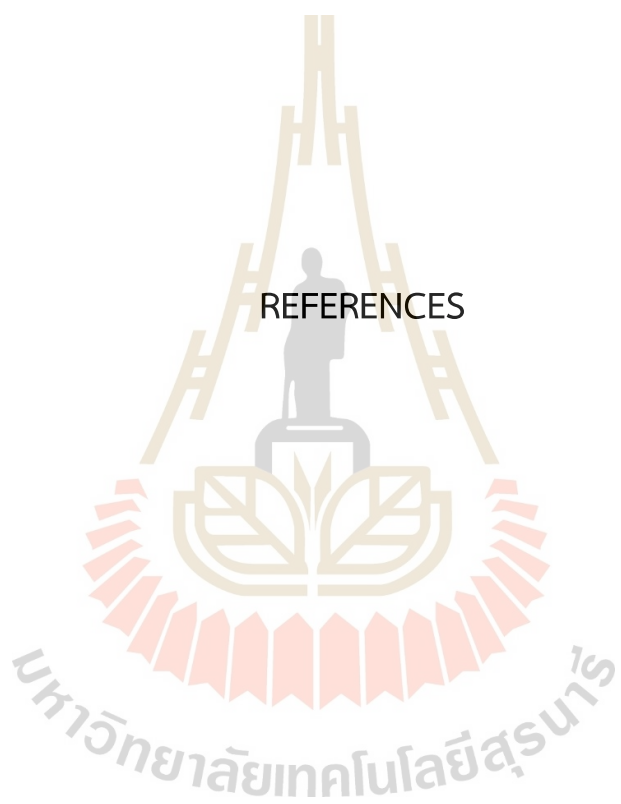
REFERENCES

Alston, W. N., Fabian, A. C., Buisson, D. J. K., Kara, E., Parker, M. L., Lohfink, A. M., Uttley, P., Wilkins, D. R., Pinto, C., De Marco, B., Cackett, E. M., Middleton, M. J., Walton, D. J., Reynolds, C. S., Jiang, J., Gallo, L. C., Zogbhi, A., Miniutti, G., Dovciak, M., and Young, A. J. (2018). The remarkable X-ray variability of IRAS 13224–3809 – I. The variability process. *Monthly Notices of the Royal Astronomical Society, 482*(2), 2088-2106. https://doi.org/10.1093/mnras/sty2527

Alston, W. N., Fabian, A. C., Kara, E., Parker, M. L., Dovciak, M., Pinto, C., Jiang, J., Middleton, M. J., Miniutti, G., and Walton, D. J. (2020). A dynamic black hole corona in an active galaxy through X-ray reverberation mapping. *Nature Astronomy, 4*(6), 597-602.

Atangana, A. (2018). *Fractional Operators with Constant and Variable Order with Application to Geo-Hydrology*. Elsevier Inc.

Bambi, C. (2018, June 01, 2018). Astrophysical Black Holes: A Compact Pedagogical Review. *Annalen der Physik, 530*, 1700430. https://doi.org/10.1002/andp.201700430

Breiman, L. (1996). Bagging predictors. *Machine learning, 24*(2), 123-140.

Breiman, L. (2001). Random forests. *Machine learning, 45*(1), 5-32.

Caballero-García, M., Papadakis, I., Dovčiak, M., Bursa, M., Svoboda, J., and Karas, V. (2020). A combined timing/spectral study of IRAS 13224-3809 using XMM–Newton data. *Monthly Notices of the Royal Astronomical Society, 498*(3), 3184-3192.

Cackett, E. M., Zoghbi, A., Reynolds, C., Fabian, A. C., Kara, E., Uttley, P., and Wilkins, D. R. (2014). Modelling the broad Fe Kα reverberation in the AGN NGC 4151. *Monthly Notices of the Royal Astronomical Society, 438*(4), 2980-2994. https://doi.org/10.1093/mnras/stt2424

Chainakun, P., Luangtip, W., Jiang, J., and Young, A. J. (2022). Mapping the X-ray corona evolution of IRAS 13224-3809 with the power spectral density. *The Astrophysical Journal, 934*(2), 166.

Chainakun, P., Mankatwit, N., Thongkonsing, P., and Young, A. (2021). Machine learning application to detect light echoes around black holes. *Monthly Notices of the Royal Astronomical Society, 506*(4), 5318-5327.

Chainakun, P. (2019, June 01, 2019). Modeling the X-Ray Power Spectra of AGN by Using Reprocessing Echoes from an Extended Corona. The Astrophysical Journal, 878, 20. https://doi.org/10.3847/1538-4357/ab1f0a

Chainakun, P., Watcharangkool, A., Young, A. J., and Hancock, S. (2019, July 01, 2019). X-ray time lags in AGN: inverse-Compton scattering and spherical corona model. *Monthly Notices of the Royal Astronomical Society, 487*, 667. https://doi.org/10.1093/mnras/stz1319

Chainakun, P., Young, A. J., and Kara, E. (2016). Relativistic X-ray reverberation modelling of the combined time-averaged and lag-energy spectra in AGN. *Monthly Notices of the Royal Astronomical Society, 460*(3), 3076-3088. https://doi.org/10.1093/mnras/stw1105

Curtis, H. D. (1918, January 01, 1918). Descriptions of 762 Nebulae and Clusters Photographed with the Crossley Reflector. Publications of Lick Observatory, 13, 9-42. https://ui.adsabs.harvard.edu/abs/1918PLicO..13....9C

Emmanoulopoulos, D., Papadakis, I., Dovčiak, M., and McHardy, I. (2014). General relativistic modelling of the negative reverberation X-ray time delays in AGN. *Monthly Notices of the Royal Astronomical Society, 439*(4), 3931-3950.

Emmanoulopoulos, D., Papadakis, I. E., Epitropakis, A., Pecháček, T., Dovčiak, M., and McHardy, I. M. (2016). A search for X-ray reprocessing echoes in the power spectral density functions of AGN. *Monthly Notices of the Royal Astronomical Society, 461*(2), 1642-1655. https://doi.org/10.1093/mnras/stw1359

Epitropakis, A., Papadakis, I. E., Dovčiak, M., Pecháček, T., Emmanoulopoulos, D., Karas, V., and McHardy, I. M. (2016, October 01, 2016). Theoretical modelling of the AGN iron line vs. continuum time-lags in the lamp-post geometry. *Astronomy and Astrophysics, 594*, A71. https://doi.org/10.1051/0004-6361/201527748

Fabian, A. C. (1999, April 01, 1999). Active Galactic Nuclei. Proceedings of the National Academy of Science, 96, 4749-4751. https://doi.org/10.1073/pnas.96.9.4749

Haardt, F., and Maraschi, L. (1991, October 01, 1991). A Two-Phase Model for the X-Ray Emission from Seyfert Galaxies. *The Astrophysical Journal, 380*, L51. https://ui.adsabs.harvard.edu/abs/1991ApJ...380L..51H

Ingram, A., Mastroserio, G., Dauser, T., Hovenkamp, P., van der Klis, M., and García, J. A. (2019, September 01, 2019). A public relativistic transfer function model for X-ray reverberation mapping of accreting black holes. *Monthly Notices of the Royal Astronomical Society, 488*, 324. https://doi.org/10.1093/mnras/stz1720

Jospin, L. V., Laga, H., Boussaid, F., Buntine, W., and Bennamoun, M. (2022). Hands-on Bayesian neural networks—A tutorial for deep learning users. *IEEE Computational Intelligence Magazine, 17*(2), 29-48.

Kara, E., Alston, W. N., Fabian, A. C., Cackett, E. M., Uttley, P., Reynolds, C. S., and Zoghbi, A. (2016, October 01, 2016). A global look at X-ray time lags in Seyfert galaxies. *Monthly Notices of the Royal Astronomical Society, 462*, 511. https://doi.org/10.1093/mnras/stw1695

Mankatwit, N., Chainakun, P., Luangtip, W., and Young, A. J. (2023). Coronal height constraint in IRAS 13224–3809 and 1H 0707–495 by the random forest regressor. Monthly Notices of the Royal Astronomical Society, 523(3), 4080-4088. https://doi.org/10.1093/mnras/stad1706

Miniutti, G., and Fabian, A. C. (2004, April 01, 2004). A light bending model for the X-ray temporal and spectral properties of accreting black holes. *Monthly Notices of the Royal Astronomical Society, 349*, 1435-1448. https://doi.org/10.1111/j.1365-2966.2004.07611.x

Nowak, M. A., and Wagoner, R. V. (1991, September 01, 1991). Diskoseismology: Probing Accretion Disks. I. Trapped Adiabatic Oscillations. The Astrophysical Journal, 378, 656. https://doi.org/10.1086/170465

Padovani, P., Alexander, D., Assef, R., Marco, B., Giommi, P., Hickox, R., Richards, G., Smolcic, V., Hatziminaoglou, E., Mainieri, V., and Salvato, M. (2017, 08/23). Active Galactic Nuclei: what's in a name? *The Astronomy and Astrophysics Review, 25*. https://doi.org/10.1007/s00159-017-0102-9

Panagiotou, C., Papadakis, I., Kara, E., Kammoun, E., and Dovčiak, M. (2022). A Physical Model for the UV/Optical Power Spectra of AGN. *The Astrophysical Journal, 935*(2). https://doi.org/10.3847/1538-4357/ac7e4d

Papadakis, I., Pecháček, T., Dovčiak, M., Epitropakis, A., Emmanoulopoulos, D., and Karas, V. (2016). Signatures of X-ray reverberation in the power spectra of AGN. *Astronomy and Astrophysics, 588*, A13.

Pedregosa, F., Varoquaux, G., Gramfort, A., Michel, V., Thirion, B., Grisel, O., Blondel, M., Prettenhofer, P., Weiss, R., and Dubourg, V. (2011). Scikit-learn: Machine learning in Python. *the Journal of machine Learning research, 12*, 2825-2830.

Reynolds, C. S. (2021). Observational Constraints on Black Hole Spin. *Annual Review of Astronomy and Astrophysics, 59*(1), 117-154. https://doi.org/10.1146/annurev-astro-112420-035022

Reynolds, C. S., and Nowak, M. A. (2003, 2003/04/01/). Fluorescent iron lines as a probe of astrophysical black hole systems. *Physics Reports, 377*(6), 389-466. https://doi.org/https://doi.org/10.1016/S0370-1573(02)00584-7

Timmer, J., and Koenig, M. (1995, August 01, 1995). On generating power law noise. *Astronomy and Astrophysics, 300*, 707. https://ui.adsabs.harvard.edu/abs/1995A&A...300..707T

Urry, C. M., and Padovani, P. (1995, September 01, 1995). Unified Schemes for Radio-Loud Active Galactic Nuclei. *Publications of the Astronomical Society of the Pacific, 107*, 803. https://doi.org/10.1086/133630

Uttley, P., Cackett, E. M., Fabian, A. C., Kara, E., and Wilkins, D. R. (2014, August 01, 2014). X-ray reverberation around accreting black holes. *Astronomy and Astrophysics Review, 22*, 72. https://doi.org/10.1007/s00159-014-0072-0

Xu, Y., Pinto, C., Bianchi, S., Kosec, P., Parker, M. L., Walton, D. J., Fabian, A. C., Guainazzi, M., Barret, D., and Cusumano, G. (2021). Wind-luminosity evolution in NLS1 AGN 1H 0707−495. *Monthly Notices of the Royal Astronomical Society, 508*(4), 6049-6067. https://doi.org/10.1093/mnras/stab2984

Zhou, X.-L., and Wang, J.-M. (2005, 2004/12/17). Narrow Iron Kα Lines in Active Galactic Nuclei: Evolving Populations? *The Astrophysical Journal, 618*(2), L83. https://doi.org/10.1086/427871

CURRICULUM VITAE

Name : Nakarin Mankatwit   **Date of Birth** : 25/06/1998

Place of Birth : Surin, Thailand

Residence : 577/13, Province Buriram, District Krasang, Sub-district Krasang, Thailand 31160.

Tel : +66-970129040, +66-902302840

Education

2017-2020 : Bachelor of Science, School of Physics, Institute of Science, Suranaree University of Technology

2020-present : Master of Science, School of Physics, Institute of Science, Suranaree University of Technology

Publication

1. Mankatwit, N., Chainakun, P., Luangtip, W., and Young, A. J. (2023). Coronal height constraint in IRAS 13224–3809 and 1H 0707–495 by the random forest regressor. Monthly Notices of the Royal Astronomical Society, 523(3), 4080-4088.

2. Chainakun, P., Mankatwit, N., Thongkonsing, P., and Young, A. (2021). Machine learning application to detect light echoes around black holes. Monthly Notices of the Royal Astronomical Society, 506(4), 5318-5327.